Rapid transformation of inorganic to organic and plant available phosphorous in soils of a glacier forefield

Egli, Markus ; Filip, Damien ; Mavris, Christian ; Fischer, Benjamin ; Götze, Jens ; Raimondi, Salvatore ; Seibert, Jan

DOI: https://doi.org/10.1016/j.geoderma.2012.06.033

Rapid transformation of inorganic to organic and plant-available phosphorous in soils of a glacier forefield

Markus Egli[1]*, Damien Filip[1], Christian Mavris[1], Benjamin Fischer[1], Jens Götze[2], Salvatore Raimondi[3], Jan Seibert[1]

[1]Department of Geography, University of Zurich, CH-8057 Zurich, Switzerland

[2]TU Bergakademie Freiberg, Institute of Mineralogy, Brennhausgasse 14, D-09596 Freiberg, Germany

[3]Dipartimento Sistemi Agro-Ambientali, Università degli Studi di Palermo, Viale delle Scienze 12, 90128 Palermo, Italy

*E-mail of the corresponding author: markus.egli@geo.uzh.ch

Abstract

Chemical weathering of rocks or sediments is extremely important for the generation of soils, for the evolution of landscape, and as a main source of inorganic nutrients for plant growth and therefore for life. Temporal trends in weathering mechanisms, plant succession and nutrients availability in cold environments can be successfully studied in soil chronosequences along a glacier forefield. In the present paper, this was carried out in the pro-glacial area of Morteratsch. Different forms of phosphorous in the soil, stream and spring water chemistry were investigated. Apatite constitutes the main source of P, but it occurs only as a minor accessory mineral phase in the granitic/gneiss parent material. The identification of apatite was performed using SEM-EDX and cathodoluminescence. Water chemistry data indicated some calcite dissolution at the earliest phase of exposure, pyrite and – on older surfaces increasingly – feldspar weathering. Apatite also seemed to contribute to Ca which is leached from the soils. The concentrations of dissolved P in the stream and spring waters were, however, extremely low (only a few µg P/l). In the topsoil, the

total stocks of P showed a slight decrease with time. Losses were rather difficult to detect even though the water fluxes through the soils and discharges are relatively high. Soil organic P is almost identical to the EDTA-extractable fraction. In an 11.5 ky-old soil outside the glacier forefield the concentration and proportions of organic P, EDTA-extractable P and inorganic P forms did not differ that much from the oldest soils (max. 150 y) of the glacier forefield. In the bulk soil, about 78% of total P was transformed into an organic form (40% already after 150 years) and, in the fine earth, about 81% (40 – 70% after about 150 years of soil evolution). Thus the P transformation reactions are shown to be very rapid, occur predominantly in the early phase of soil formation, and could be best described by an exponential decay model.

Keywords: Phosphorous, glacier forefield, weathering, apatite, initial soils

Introduction

Since approx. 1850 AD, most Alpine glaciers show phases of marked recessions, temporarily interrupted by smaller glacier advances (Furrer, 1991; Maisch, 1992; Holzhauser and Zumbühl, 1996). Locally, large deglaciated surfaces arose where vegetation development, i.e. primary plant succession, could start. The glacier forefield is in most cases defined as the area between the present-day glacier extent and the distinct moraines deposited in the 1850s. Soils in pro-glacial areas in the Alps are, consequently, young and were formed over a time-span of about 150 years (the time since the end of the ‘Little Ice Age’ in the 1850s; Fitze, 1982). As a consequence of warming, additional areas will become ice-free and subject to weathering and soil formation.

Alpine glacier forefields provide unique opportunities to study initial soil formation, nutrient availability and plant successions along the chronosequences and consequently the development of life. Biogeochemical weathering processes in such environments initiate the mobilisation of biolimiting nutrients (phosphorus, iron, potassium, calcium) and give rise to primary production (Föllmi et al., 2009). Plant succession is highly influenced by the underlying substrate, its weatherability and other site factors. Anderson et al. (2000) and Matthews and Whittaker (1987), for instance, showed that factor complexes like snow melt, exposure, moisture, terrain and time

control vegetation succession. However, only few studies deal with the substrate characteristics (parent material and soils) in pro-glacial areas and little is known about the rates of physical and chemical changes of soils in such areas and their consequences for plant growth. Several authors (Egli et al., 2003; Hosein et al., 2004; Föllmi et al., 2009; Mavris et al., 2010 etc.) suggested that glacially-derived material is subjected to enhanced chemical weathering, starting immediately after deposition in the pro-glacial zone and subsequently continuing for thousands of years after glacier retreat. The pro-glacial area is a potential zone of high geochemical reactivity due to the availability of freshly-ground reactive material (subglacially derived), often high water:rock ratios and contact times, high permeabilitiy and a constant supply of dilute waters (meltwater and rain/snowmelt) to percolate through the deposits (Föllmi et al., 2009).

The weathering of phosphorus-bearing minerals in rock substrata and the subsequent release of P to soils and the aqueous environment is considered as the principal mechanism by which P is transferred from the lithosphere to the biosphere (e.g., Filippelli, 2008; Föllmi et al., 2009). The release of directly or potentially bioavailable P to the biosphere represents a key factor in driving primary productivity rates. According to Föllmi et al. (2009), cycles of glaciation-deglaciation may reactivate transport-limited weathering regimes by replacing old and deeply-weathered soils with immature pedospheres, in which the dissolution of glacially-derived detrital P proceeds rapidly and in which bioavailable P is efficiently transferred into the biosphere.

Availabilities of nitrogen (N) and phosphorus (P) are important determinants of primary ecosystem succession. On areas that have only recently been deglaciated, inorganic forms of N and P predominate, which originate either from parent rock weathering and/or deposition (Welc et al., 2010).

The aim of our study was consequently to see how quickly inorganic P is transformed in a glacier forefield exhibiting young soils at an initial stage of development into other chemical forms such as organic or plant-available P and whether such transformation processes are bound to a loss (leaching) of phosphorous. For this purpose, weathering mechanisms had to be studied and, therefore, both soil and water analyses had to be taken into account.

Investigation area

The investigation area is the glacier forefield of Morteratsch in the Upper Engadine (Swiss Alps). The backwall of the glacier is formed by high mountain peaks of the South Raetian Alps, such as Piz Bernina (4049m asl.) and Piz Palü (3901m asl). The surrounding region of Morteratsch belongs to the Lower Austroalpine Bernina Nappe that comprises mainly various plutonic rock types, like granodiorites and alkali-granites, and subordinate syenites, diorites and gabbros (Büchi, 1994; Spillmann, 1993). The border of the pro-glacial area is given by terminal moraines deposited in the 1850s during the 'Little Ice Age' (Fig. 1). The actual length of this pro-glacial area is approx. 2 km and has an area of 1.8 km^2. The pro-glacial area is in a valley that runs N-S. The altitude ranges of the area of interest were between 1900 m asl to about 2050 m asl. The Swiss Glaciological Commission of the Swiss Academy of Natural Sciences scnat (Gletscherberichte, 1881–2008) recorded historical and recent glacier length fluctuations (Fig. 1; see also Maisch et al., 1993).

Alpine glaciers have fluctuated during the last 10 – 12 ky near the terminal moraines formed in the year 1850. This has been shown by many geomorphologic and climatic studies (cf. Patzelt, 1977; Fitze, 1982; Gamper, 1985; Magny, 1992; Maisch, 1992;). Consequently, the exposure age or the age of soils outside the glacier forefield increases very abruptly.

The glacial till in the glacier forefield consists of granitic and gneissic material and was produced through glacial transport within a small area of relatively homogeneous parent material. The dominant soil units (some areas even do not have a soil) in the pro-glacial area are Haplic Fluvisols, Endoskeletic, Skeletic or Lithic Leptosols, Humi-skeletic Leptosols (Fig. 1), including some sites with Rankers that have a weak B horizon (IUSS working group, 2007), and, very rarely, Dystric and Endogleyic Cambisols (endoskeletic). The young soils that are close to the glacier showed almost no morphologic signs of chemical weathering and alteration products.

Primary plant succession of the pro-glacial area with its predominantly silicatic parent material starts with the pioneer plant communities Oxyrietum digynae and Epilobietum fleischeri and ends with the larch/Swiss stone pine forest (Larici-Pinetum cembrae) after substantially more than 150 years (Burga et al., 2010). The first plants, i.e. *Epilobium fleischeri, Oxyria digyna, Linaria alpina*, *Saxifraga aizoides*, *Rumex scutatus* appear about 7 years after deglaciation and reach greater cover-abundance values (about 5 – 25%) after about 27 years (Burga et al., 2010). The first

species of the short-living Oxyrietum digynae appears approx. 10 years after deglaciation and disappears approx. 30 years later. The first shrubs of willows, green alder, dwarf-shrubs and small larch trees are found on areas that have been ice-free for about 12 to 15 years. The establishment of *Larici-Pinetum cembrae* takes place after about 77 years.

Present-day climatic conditions for the Morteratsch site are approx. 0.5 °C mean annual air temperature and approx. 1000 – 1300 mm mean annual precipitation as calculated by using data from the nearby meteorological stations Samedan and Bernina.

Over the period 2003–2007 mean daily discharge has been in the region of 4 – 5 m^3/s, but the 2003–2007 July mean daily discharge was 11.2 m^3/s with a maximum of 85 m^3/s on 9 July 2004 (Stott et al., 2008). The Ova da Bernina is part of the catchment of the River Inn, which is the major Alpine tributary of the upper Danube. A further 4 km downstream at Pontresina, the Swiss Federal Office for the Environment has maintained a gauging station since 1955 (No. 2262 Berninabach–Pontresina, 46°29'06"N, 9°54'35"E) at an altitude of 1804 m asl which drains a catchment area of 107 km^2, approximately 47% of which is snow- and ice-covered in summer (Stott et al., 2008).

Materials and methods

Soil and water sampling

Surface soil samples (topsoils, A or AO horizon; soil depth usually between 0 to 5/10 cm) were collected from the whole pro-glacial area (Fig. 1) forming a soil chronosequence ranging from 0 to 150 y. Ten of these sites were close to the monitoring sites of Mavris et al. (2010). Additional sites were sampled close to the glacier (sites B1 – B4) as well as another one (site AP) outside the pro-glacial area on a surface having an age of about 11.5 ky (Egli et al., 2003).

Around two kilograms of soil material were collected per sample. In order to yield reasonable results, large soil sampling volumes are needed for soils in alpine areas (Hitz et al., 2002). Soil bulk density was determined by a soil core sampler (or by excavated holes having a volume of about 500 – 2000ml that were backfilled with a measurable volume of quartz sand).

Four different types of water were considered: spring water and tributary water in the glacier

forefield (SW); and ice water (ICE), glacial stream water (GWa, GWz, BO1) and tributary water outside the glacier forefield (TW). The two streams outside the pro-glacial area (TW) were sampled to compare waters from young and older surfaces. The surface outside the pro-glacial area has a much older age (10 – 15 ky; Fitze, 1982) than the pro-glacial area (maximum age = 150 y).

Water was collected during the summer periods of 2008 – 2010 (June – September), 2 – 5 times per sampling season. All sampling bottles were acid washed (HNO_3 1M) and rinsed with double distilled water to prevent contamination.

All water samples were either collected in PE- or glass (for $\delta^{18}O$ and $\delta^{2}H$) vials filtered with 0.45 μm pre-cleaned millipore filters to eliminate suspended particles and stored in the dark at 4 °C.

Chemical, physical and mineralogical analyses

Electric conductivity of the water, pH, HCO_3^- and temperature were measured directly in the field. Water-pH was measured using a field pH-meter Metrohm E 604, conductivity using a microprocessor conductivity meter (LF320) having the standard conductivity cell (TetraCon 325) and HCO_3^- was determined by titration (using HCl).

Ca, Mg, K, Na and Sr were analysed by an AAS (Perkin Elmer Atomic Absorption Spectrometer) using graphite furnace for the Sr measurements. The anions Cl^-, NO_3^-, SO_4^{2-} and PO_4^{3-} were analysed using an ion chromatograph Metrohm 733 IC Separation Centre. Silicon was measured photometrically. In addition, some samples were analysed for Al, Ba, Fe, P, Si, Sr using inductively-coupled plasma optical emission spectrometry (ICP-OES; PE 3300DV). Charged organic compounds were derived from the difference of the equivalent sum of cations and anions.

The measurements of $\delta^{18}O$ and $\delta^{2}H$ were performed using a Cavity Ring-Down Spectroscopy (CRDS) Picarro L1102i liquid analyser (manufactured by PICARRO). The device was connected to a LC PAL liquid auto-injector (CTC Analytics AG, Zwingen, Switzerland), equipped with a 1.2 µl syringe (model 26P/-mm/AS, 7701.2 N CTC manufactured by the Hamilton Company of Reno, Nevada, USA) for the injection of water samples into the machine. Samples and standards were injected into 32 x 11.6 mm screw neck 1.5 ml vials filled with 1 ml of water having PTFE/silicone/PTFE septums. The analysis scheme was based on two laboratory standards calibrated with Standard Light Antarctic Precipitation (SLAP) and Vienna Standard Mean Ocean

Water (VSMOW) used for interpolation and a control laboratory standard not included in the calibration. The regression between measurements and known δ values for calibration standards was used to convert the measured absolute isotopic ratios to delta values.

$$\delta^{18}\mathrm{O} = \left(\frac{{}^{18}\mathrm{O}/{}^{16}\mathrm{O}(sample)}{{}^{18}\mathrm{O}/{}^{16}\mathrm{O}(STD)} - 1 \right) \times 1000 \qquad (1)$$

Total C and N contents of the soil and parent material were measured using a C/H/N analyser (Elementar Vario EL). Soil pH (in 0.01 M $CaCl_2$) was determined on air-dried fine earth samples using a soil:solution ratio of 1:2.5.

The particle-size distribution was determined on some selected soil samples. After a pre-treatment of the samples with H_2O_2 (3%), particle-size distribution of the soils was measured using a combined method consisting of sieving out the coarser particles (2000 – 32µm) and the measurement of the finer particles (< 32µm) by means of an X-ray sedimentometer (SediGraph 5100).

Element pools in the soil (Ca, Mg, Na, K, Si, Fe, Al, Ti, and Mn) were determined by a total dissolution method for the parental material (Table 1). Oven-dried samples were dissolved using a mixture of HF, HCl, HNO_3, and H_3BO_3 (Hossner, 1996) in a microwave oven and at a pressure of c. 25 bar in a closed system. Concentrations were measured using a Perkin Elmer Atomic Absorption Spectrometer (AAS). The NH_4OAc-EDTA extractable fraction of phosphorous (plant available fraction) was measured according to Lakanen and Erviö (1971). Concentrations were determined photometrically at wavelength 692 nm using ammonium molybdate. Total P in the soils was determined using H_2SO_4 after heating the samples to 550°C (Kuo, 1996) while the inorganic P fraction was determined on unheated samples. The organic fraction was determined as the difference between total and inorganic P.

Due to the low occurrence of apatite, XRD was not the appropriate technique with which to detect it. Therefore, scanning electron microscopy (SEM) coupled with an energy-dispersive spectroscopy (EDX) and cathodoluminescence (CL) was used as an alternative. CL measurements were carried out using a hot cathode CL microscope HC1-LM (Neuser et al., 1995). The system was operated at 14 kV accelerating voltage and a current density of about 10 µA/mm^2.

Luminescence images were taken on-line during CL operations using a Peltier cooled digital video-camera (KAPPA 961-1138 CF 20 DXC). CL spectra were recorded in the wavelength range 320 to 900 nm using an Acton Research SP-2356 digital triple-grating spectrograph with a Princeton Pixi 256B Spec 10 CCD detector that was attached to the CL microscope by a silica-glass fibre guide. CL spectra were measured under standardised conditions (wavelength calibration by a Hg-halogen lamp, spot width 30 μm, measuring time 1 – 5 s). The measurements were carried out at the TU Bergakademie Freiberg, Germany.

The analysis with SEM-EDX was performed using a Dual Beam Quanta 200 3D FEI, with Dual BSD detector and W emitter operating at an accelerating voltage of 20 kV. Investigations were performed at the Institute for Building Materials (ETH Zurich, Switzerland).

Statistics

The soil and water datasets were checked for normal distribution using a Shapiro-Wilk test (SigmaPlot 11.0 (Systat Software Inc.); Jann, 2005). This procedure was applied using a two-tailed test for significance. The datasets usually did not show a normal distribution. Consequently, the Spearman rank correlation coefficient was taken.

Results

Soils

Some main soil characteristics are given in Table 2. In general, they all show only a (very) weak weathering stage and are characterised as sand to sandy loam. The total phosphorous concentrations were in the range of about 160 to 820 mg/kg and varied considerably along the chronosequence in the glacier forefield (Fig. 2). A temporal trend (accumulation or depletion) could not be observed. Also outside the pro-glacial and in a much older soil (about 11.5 ky), the P concentration was still in a similar range.

However, if the inorganic and organic P fractions are compared, temporal changes then seem to be obvious. Already within 150 years of soil evolution, a marked decrease of the inorganic P

fractions could be detected while the organic fraction seems to be mirror-inverted. After about 150 years, at least half of the inorganic P fraction in the fine earth had been transformed into an organic P form (Fig. 2). The EDTA-extractable fraction (which includes the exchangeable fraction, organically-bound species and species adsorbed on oxyhydroxides; cf. Miller et al., 1986; Keller and Védy, 1994) of phosphorous seemed to be almost identical to the organic fraction. Similarly to the organic fraction, the EDTA-extractable P increased with the age of the soils (Fig. 3): after about 150 years, also this fraction included about 50% of the total phosphorous.

An estimate of the stocks of the individual P fractions in the fine earth and bulk soil (including soil skeleton) was performed using the following equations:

Fine earth: $$\mathrm{P}_{stock,FE} = \mathrm{P}_i d_i \rho_i (1 - RM) \quad (2)$$

Soil skeleton: $$\mathrm{P}_{stock,SK} = \mathrm{P}_i d_i \rho_i RM \quad (3)$$

Bulk soil: $$\mathrm{P}_{stock} = \mathrm{P}_{stock,FE} + \mathrm{P}_{stock,SK} \quad (4)$$

where P_{stock} denotes the P abundance (g/m^2) in the fine earth (*FE*) or soil skeleton (*SK*), P_i the concentration of the fraction *i* (g/t), d_i the soil depth (0.05m), ρ_i = soil density (t/m^3) and *RM* the mass proportion of soil skeleton (diameter > 2mm).

The stock calculations were related to a unit depth of 5 cm (as most soils were very weakly developed and had an A, OA or O horizon of about that depth): for this purpose, also the soil skeleton fraction for each soil had to be measured.

The total P stocks in the fine earth were usually in the range of 5 – 25 g/m^2 to the depth of 5 cm depth (Fig. 4) and did not change over time. After about 100 years of soil evolution, the proportion of the organic P fraction sharply increased and reached after 10ky about 81% of the total fine earth mass. If the soil skeleton fraction is included in these calculations, then the P stocks usually varied in the range of 20 – 35 g P/m^2 to the depth of 5 cm depth. With time, around 78% of the total P was transformed into organic P (Fig. 4). The total P stocks (including the soil skeleton) in the topsoil seemed, however, to decrease slightly within the considered time span of 11.5 ky.

The chemical (Table 1) and also the mineralogical composition (Table 3) of the soil material typically reflected its granitic origin. Quartz, K-feldspar and Na-rich plagioclase were determined as the most abundant phases, followed by Fe-rich mica (biotite) and epidote. Using

cathodoluminescence, apatite could be detected – in the parent material or very young soils and in the older soils in the glacier forefield (Fig. 5). Apatite, characterised by euhedral crystals with mostly a size of about 30 μm (but in some cases up to almost 1 mm), sporadically occurred in the glacial till. Apatite had a strong yellow luminescence emission (Fig. 5). The diadochic substitutions within the apatite clearly reflected the geology of the granitoid bedrock (see, e.g. Zhang et al., 1985; Kempe and Götze, 2002). The investigated samples did not feature any rim (or growing) structures in the crystal, which is typical for a homogeneous composition of apatite.

Water analyses

The overall mineralisation of the waters was generally rather low. The total amount of dissolved compounds was in the range of 5 x 10^{-5} to 1 x 10^{-3} mol/l. The mineralisation degree and the $\delta^{18}O$ values confirmed that the water originated from the glacier-catchment and that the residence time in the subsurface is low. The dominant cation in the spring and stream waters (usually more than 50% of the equivalents of the positively-charged ions) was Ca^{2+} (Fig. 6). The other cations (Mg^{2+}, K^{+}, Sr^{2+}) were measured in low concentrations while Na^{+} was slightly more abundant. HCO_3^{-} and SO_4^{2-} dominated the anions. Cl^{-} and NO_3^{-} were present in concentrations < 0.4 $mmol_c/dm^3$. The lowest concentrations were, not surprisingly, measured in the ice-water (small stream on top of the glacier) that consists purely of ice and snow melting water.

In general, a (temporal) shift of the chemical composition was measured when correlated to the age of the surface. Ice water predominantly consisted of Ca^{2+}, HCO_3^{-} and some Cl^{-} and NO_3^{-} whereas the stream and spring-water in the glacier forefield and particularly the tributary waters outside the glacier forefield became enriched in K^{+} and Na^{+}. Consequently, the older the surface the higher is the relative abundance of K^{+} and Na^{+}. On very young surfaces, the water composition reflected more calcite (or epidote) weathering and on older surfaces more plagioclase, alkali feldspar and/or sheet silicates weathering. The increasing importance of silicate weathering with surface age is also documented in the dissolved Si concentrations that steadily increased with distance from the glacier (Fig. 7).

The phosphate concentration was always below the detection limit (100 µg/l) using Ion-Chromatography (the routinely-used method). Only a few micrograms of P were detectable in

water using ICP-OES (Fig. 8). There may well even be a tendency of decreasing P concentrations with increasing distance from the glacier snout; however, the number of observations was too low for establishing a statistically-relevant trend.

Hydrology

The $\delta^{18}O$ and $\delta^{2}H$ are compared in Figure 9. All values are near the 'Global Meteoric Water Line' (GMWL; Aggarwal et al., 2005) and the 'Local Meteoric Water Line' (LMWL). A better correlation is, however, achieved using the LMWL. For northern Switzerland a LMWL was derived with the equation $\delta^{2}H = 7.55 \times \delta^{18}O + 4.8$ (Pearson, 1991). Compared to the GMWL, the LMWL and consequently the measured samples indicated a more continental climate. The $\delta^{18}O$ and $\delta^{2}H$ values are, however, also influenced by seasonal variations (cf. Hindshaw et al., 2011), because the melting of ice and snow influences the water residence time and the water composition. The ice-water (melting water from the glacier surface), collected close to the glacier snout, usually had distinctly less negative $\delta^{18}O$ and $\delta^{2}H$ values than the glacial stream. This particular ice-water had a very local origin. With decreasing altitude, the $\delta^{18}O$ becomes less negative (Pearson, 1991). Compared to the ice-water that derived from locally melting water (collected on top of the glacier front), the more negative values of the glacial stream consequently mean that a significant part of the waters derives from higher altitudes. The glacier front was at an altitude of about 2050 m asl and the hydrologic catchment reaches altitudes of up to 4000 m asl. The oxygen isotopes were measured twice in 2010 (August and September). For both sampling campaigns, the $\delta^{18}O$ became less negative as a function of distance from the glacier front. The slight increase in the $\delta^{18}O$ ratio in the pro-glacial area consequently means that the stream water receives some contribution from tributary waters and/or precipitation. From the measured $\delta^{18}O$ increase within the pro-glacial area (~ 0.3‰), this contribution can be estimated to have a maximum value of c. 20%. The change in $\delta^{18}O$ could be also due to weathering; however, the water dilution effect is most likely too high and overshadows potential weathering effects. A correlation analysis of $\delta^{18}O$ with all the different solutes did not reveal any significant relationship. However, our $\delta^{18}O$ dataset is small and further data would be necessary to provide conclusive findings.

Discussion

Soil formation and weathering progress rapidly in the glacier forefield of Morteratsch (Mavris et al., 2012). Due to the increasing vegetation cover with age of surface exposure and higher plant productivity, more organic carbon is transferred into the soils as they develop (Table 2). This affects weathering and consequently also the transformation of the phosphorous forms.

In granitic catchments, carbonate leaching is often seen as a major source of Ca (e.g. White et al., 1999a,b; Hosein et al., 2004). The investigated waters (springs, glacial stream, and rivers outside the pro-glacial area) are, however, strongly undersaturated with respect to calcite and dolomite (Mavris et al., 2010). Thus, the behaviour of Ca^{2+} and Mg^{2+} cannot be explained by only these two mineral phases. The solubility of Ca and Mg is also kinetically controlled by Ca- and Mg-bearing phases (silicates, phosphates). The dissolution of apatite represents a potential source of Ca (Blum et al., 2002). The correlation analysis showed that a certain relation – however not overwhelmingly significant – exists between Ca^{2+} and PO_4^{3-} (Table 4).

The runoff water reflects the geochemical processes in the glacier forefield. The main mineral dissolution reactions are (see also Mavris et al., 2010; Table 4):

Calcite (representing carbonates)

$$CaCO_3 + CO_2 + H_2O = Ca^{2+} + 2HCO_3^- \quad (5)$$

Plagioclase (representing tectosilicates):

$$Ca_xNa_{(1-x)}Al_{(1+x)}Si_{(3-x)}O_8 + (1+x)CO_2 + (2 + 2x)H_2O$$
$$= xCa^{2+} + (1-x)Na^+ + (3-x)SiO_2 + (1+x)HCO_3^- + (1+x)Al(OH)_3 \quad (6)$$

where x is the Ca-rich component (White at al., 1999b).

Apatite (phosphate):

$$Ca_5(PO_4)_3OH + 7\ H^+ = 5\ Ca^{2+} + 3\ H_2PO_4^- + H_2O \quad (7)$$

Elevated Ca/Si ratios e.g. Ca/ Si=12 (Anderson et al., 2000; Bench River) are thought to be caused by calcite dissolution. In general, calcite dissolution is a main supplier of Ca. However, this ultimately also depends on the amount of calcite present in the parent material. The bedrock or parent material contained very little calcite (Table 3). The Ca/Si ratios in the water usually were in

the range of 0.7 – 7 and consequently higher than in the Damma glacier forefield (Hindshaw et al., 2011). Therefore, some calcite dissolution is likely, but other Ca-bearing (unstable) minerals such as hornblende, plagioclase or apatite also have to be taken into account as possible Ca sources (Fig. 6). Sulphate significantly correlated with the major cations. Some pyrite (as a minor constituent of the parent material) armoured by calcite was also observed in the pro-glacial area. The good correlation between SO_4^{2-} and Ca^{2+} most likely indicates the contemporaneous dissolution of pyrite and carbonates.

In addition, biological processes contribute to element leaching from rocks and soils. The dissolved and charged organic compounds correlated with all major cations (Table 4). As reported by Brunner et al. (2011), pioneering fungi in a glacier forefield are able to dissolve the granite by releasing a variety of organic acids such as citric, malic and oxalic. In some cases, it was reported that mycorrhizal fungi produced oxalic acid that finally promote weathering (e.g. Hoffland et al., 2004; van Schöll et al., 2008). In particular Si and K mobilization might be affected by the presence of mycorrhiza (van Hees et al., 2006). Jongmans et al. (1997) showed that ectomycorrhizal fungi drill innumerable narrow cylindrical pores (diameter 3–10 μm) into weatherable minerals in podzol E horizons. The fungi probably form micropores by exuding strongly complexing low-molecular weight organic acids at their hyphal tips, causing highly local dissolution of silicates. Ectomycorrhizal (EM) fungi are known to colonize minerals in forest soil, and in many laboratory experiments it has been confirmed that EM fungi stimulate dissolution of minerals such as apatite, biotite and feldspars (Wallander and Hagerberg, 2004). Glacial deposits are at the beginning often depleted of symbiotic fungi but colonized by them over time after exposure (Cázares et al., 2005). Also weathering-associated bacteria produce oxalic acid or HCN (Frey et al., 2010). Frey et al. (2010) and Brunner et al. (2011) concluded that fungi and bacteria colonisation of young, granitic surfaces play a crucial role in the initial soil formation in previously glaciated mountains.

Furthermore, one has to consider that the streamwater chemistry in glacier forefields may be strongly controlled by glacial melting and the routing of this glacial melt water through the glacier, resulting in marked seasonal and even diurnal variations (Hindshaw et al., 2011).

The progressive dissolution of apatite is the basic mechanism controlling the release of inorganic P in the newly-forming soil and also contributes to the availability of Ca for plants. Minor amounts of

P can probably be released by the decomposition of feldspar minerals. According to Smith (1983), feldspar minerals contain 0.00x-0.0x % P. Using cathodoluminescence, apatite could be detected (while this was not the case using XRD and DRIFT measurements) due to its bright yellow CL (Mn^{2+} activation). The intensity of the luminescence is strongly orientation-dependent (Finch et al., 2003) and variation in luminescence can be linked to crystallographic controls (i.e. Barbarand and Pagel, 2001). In both samples, the parent material and the oldest soil of the glacier forefield, the presence of apatite could be verified.

Following dissolution from apatite, P is generally retained in Fe oxyhydroxides and organic matter (cf. Nezat et al., 2007). Also in this case, a significant correlation between the oxalate-extractable Fe and the EDTA-extractable P could be found ($R^2 = 0.61$; $p < 0.05$; Table 5). The Fe in biotite, when present, may also immediately lock up all of the P (Nezat et al., 2007). Föllmi et al. (2009) showed that with time organic- and iron-bound P almost completely replace detrital P. Apatite should be easily dissolved in surface waters due to its relatively high dissolution rate compared to silicate minerals. The solubility of P was, however, very low and the concentrations remained in the range of a few micrograms per litre. Also Hindshaw et al. (2011) measured very low (below the detection limit) P concentrations of < 50 µg/l in the stream waters in the Damma glacier catchment. As soils develop, primary apatite is weathered from the soil. The released Ca is taken up by vegetation, held on the exchange complex, or dissolved in groundwater and lost from the ecosystem. In contrast, P is comparatively immobile (Wood et al., 1984; Nezat et al., 2007) and, after being released by weathering, is retained in the soil complexed by organic matter and secondary minerals (Walker and Syers, 1976; Cross and Schlesinger, 1995), resulting in a relatively constant P concentration above the C horizon (Nezat et al., 2007). A rather weak correlation (error probability < 0.1) of organic and EDTA-extractable P to pH exists whereas the org. C content obviously does not have a great effect on P speciation (Table 5). The decrease in pH (that is bound to calcite dissolution and the leaching of base cations) and the low effect of total organic C on P speciation shows that bacteria and fungi (including mycorrhiza), by the release of organic acids, are most likely decisive for the availability of phosphorous for plant growth (Jongmans et al., 1997; Frey et al., 2010).

The transformation of inorganic P forms into organic ones was a very rapid process and mainly occurred within 150 years of soil evolution in the glacier forefield of Morteratsch. The chronofunctions of the organic and EDTA-extractable P concentrations in the topsoil were best fitted to data using the exponential decay model (Fig. 3). The exponential decay model (cf. Lichter, 1998) is given by

$$f(t) = a + (b - a)e^{-kt} \quad (8)$$

where *a* represents an asymptote, *b* the initial quantity, and *k* the decay constant. Steady state conditions seem to be reached after about 100 – 200 years. A similar behaviour could be observed for the organic and inorganic P fraction (Fig. 4) where very rapid changes were measured and relatively soon an asymptotic end value seemed to be reached. The general behaviour and shape of the tendency seem to be similar to other components that have been measured in Alpine chronosequences (see Dahms et al., 2012).

Our data suggest that only a small part of P is lost due to leaching or weathering processes (Fig. 4) and that nearly all P cycles within the bio-geosphere – in contrast to many major ions that are leached with weathering. The decrease of the total P stocks (fine earth and soil skeleton included; Fig. 4C) in the topsoil within 150 years is however just slightly under the level of being statistically significant ($p = 0.054$; $R = -0.52$). Over 11500 years however, the error probability is slightly below 5% ($p = 0.03$; $R = -0.56$) and the decrease consequently significant for total P in the topsoil. A part of this loss might be apparent, because with time bulk density and consequently the soil mass per unit area may change.

Phosphorous is very rapidly taken up by the plants, transferred back to the soil, retained and transformed (also microbiologically) into an organic form (Fig. 4B and D). A similar observation was also made by Tamburini et al. (2011) who showed that P is integrated in the soil by the microbial community; a process that begins very early in the soil development. It is also known form other investigations that organic matter accumulation is another P storage mechanism (see e.g., Bruland and Richardson, 2006). A low pH and a high content of Al and Fe oxihydoxides and organic matter were found to promote the phosphate sorption in European alpine soils (Kana et al., 2011). Our results, however, are in contrast to those of Eger et al. (2011) who measured rapid losses of total phosphorous at a rate of 110 g m^{-2} ky^{-1} on sand dunes in a super-humid climate

(3455 mm annual precipitation) in the South Island of New Zealand. In this case, apatite was also the main P source. The rapid loss of apatite-P of over 50% after only 370 y of pedogenesis was almost completely offset by the rapid accumulation of organic P in the topsoil and subsoil. The inability of pedogenesis to sustain this transformation beyond 370 y of soil evolution resulted in a steep decline of P(tot). For Morteratsch, we can do the following calculations: assuming that the mean measured P-concentration in the waters (6µg/l) represents reality and that about 500 – 700 L water/m^2 percolate the soils each year, then a loss of 3 – 4.2 g m^{-2} ky^{-1} should be the result. Given the variability of total P in the soils (25 – 40 g P m^{-2} per 5 cm depth), such a loss would be almost non-detectable even after 1000 years of soil evolution. However, after about 10 ky of soil evolution and using these calculations, the P-stock in the soil depth 0 – 5 cm should be close to zero.

Long-term weathering rates of soils can also be derived using immobile element contents as indicators and the total content of the elements of interest (Table 6; Egli and Fitze, 2000). Ti was used as an immobile element. The parameter $\tau_{j,w}$ represents the open-system mass transport function and is defined as:

$$\tau_{j,w} = \frac{C_{j,w}C_{i,p}}{C_{j,p}C_{i,w}} - 1 \qquad (9)$$

where $C_{j,p}$ (kg/t) is the concentration of element *j* in protolith (e.g., unweathered parent material, bedrock), $C_{j,w}$ is the concentration of element *j* in the weathered product (kg/t), $C_{i,p}$ (kg/t) the concentration of the immobile element *i* in the protolith (e.g., unweathered parent material, bedrock) and $C_{i,w}$ the concentration of the immobile element *i* in the weathered product (kg/t). The open-system mass transport function calculates relative losses or gains. Absolute mass changes can be determined using the following equation:

$$\bar{m}_{j,flux(z_w)} = \sum_{a=1}^{n} C_{j,p}\rho_p \left(\frac{1}{\varepsilon_{i,w}+1}\right)\tau_{j,w}\Delta z_w \qquad (10)$$

with $\varepsilon_{i,w} = \left(\frac{\rho_p C_{i,p}}{\rho_w C_{i,w}}\right) - 1$

where $\varepsilon_{i,w}$ represents the strain, ρ_p and ρ_w the bulk density (t/m^3) of the protolith and the weathered soil, respectively, n = soil layers and Δz to the weathered equivalent of the columnar height (m) of a representative elementary volume.

The relative losses and gains ($\tau_{j,w}$) for the oldest soil (Albic Podsol; 11.5 ky) are given in Figure 10. In contrast to the above-shown mass calculations (Fig. 4A and C), this approach considers also volume changes of the soil profile during its evolution ($\varepsilon_{i,w}$). Due to podsolisation, Al, Fe and also base cations are strongly leached. Consequently $\tau_{j,w}$ is negative down to the C horizon. This is typical for alpine and (strongly) weathered soils (see e.g. Egli et al., 2001). Phosphorous, however, has strongly positive values, except in the E horizon (strongly negative values due to the podsolisation effect). Two different variants (having a different starting point: C or BC horizon) were calculated – but in both cases a similar result was obtained. Phosphorous was not removed from the soil system. Although $\tau_{j,w}$ is partially strongly positive, the total added amount of P over the time range of 11.5 ky is rather low: 10 – 39 g/m^2 in the depth range of 0 – 25 cm and about 100 – 250 g/m^2 over the whole profile. This again shows that losses over a long period of time must be minimal. In our case, either some aeolian contributions or some inhomogeneities within the granitic parent material overshadowed a potential P loss. In contrast to sites showing substantial erosion effects (cf. Föllmi et al., 2009) and a subsequent loss in detrital P, sites at stable topographic positions did not evidence a measurable loss, even after 11.5 ky.

As phosphorous strongly recycles within the vegetation and given the fact that with time the roots penetrate to greater soil depths, some phosphorous will be transferred back by litter to the topsoil which may therefore mask a potential P-leaching from the soils. Furthermore, with time more Fe-oxyhydroxides that strongly retain phosphorous are formed in the soil (Nezat et al., 2007). Extrapolating roughly the hydrology of the New Zealand sites (Eger et al., 2011) to Morteratsch (by increasing the percolation rate through soils to about 2800 l/m^2), then the P loss rates would be around 17 g m^{-2} ky^{-1} to a depth of 5 cm depth and, consequently, still almost one order of magnitude lower than that measured by Eger et al. (2011).

Conclusions

Phosphorous, as an intrinsic component for the development of life, is very quickly transformed from inorganic into organic and plant-available forms. Within a time span of about 150 years of soil formation in a glacier forefield, almost half of the inorganic fraction is made available for plant growth. Apatite as the main P source (but still as a minor mineralogical component of the soil and parent material) was detectable in very young soils and also after 150 years of weathering. Leaching and consequent losses of P by percolating water through the soils seem to be very low: however, this is not the case for other major ions and nutrients such as Ca, Mg, K and Na.

Acknowledgements

This research was supported by the Swiss National Foundation (SNF) project grant n. 200021-117568. We would like to thank B. Kägi and C. Schreiner for their help in the laboratory. We are, furthermore, indebted to A. Mirabella and an unknown reviewer for their helpful comments on an earlier version of the manuscript.

References

Aggarwal, P.K., Gat, J.R., Froehlich, K.F., 2005. Isotopes in the Water Cycle. Past, Present and Future of a Developing Science. IAEA. Springer, Dordrecht.

Anderson, S.P., Drever, J.I., Frost, C.D., Holden, P., 2000. Chemical weathering in the foreland of a retreating glacier. Geochimica et Cosmochimica Acta 64, 1173-1189.

Armbruster, T., Bonazzi, P., Akasaka, M., Bermanec, V., Chopin, C., Gieré R., Heuss-Assbichler, S., Liebscher, A., Menchetti, S., Pan, Y., Pasero, M., 2006. Recommended nomenclature of epidote-group minerals. European Journal of Mineralogy 18, 551-567.

Barbarand, J., Pagel, M., 2001. Cathodoluminescence study of apatite crystals. American Mineralogist 86, 473-484.

Blum, J.D., Klaue, A., Nezat, C.A., Driscoll, C.T., Johnson, C.E., Siccama, T.G., Eagar, C., Fahey, T.J., Likens, G.E., 2002. Mycorrhizal weathering of apatite as an important calcium source in

base-poor forest ecosystems. Nature 417, 729-731.

Büchi, H. 1994. Der variskische Magmatismus in der östlichen Bernina (Graubünden, Schweiz). Schweizer Mineralogische und Petrographische Mitteilungen 74, 359-371.

Burga, C.A., Krüsi, B., Egli, M., Wernli, M., Elsener, S., Ziefle, M., Mavris, C., 2010. Plant succession and soil development on the foreland of the Morteratsch glacier (Pontresina, Switzerland): Straight forward or chaotic? Flora 205, 561-576.

Bruland, G.L., Richardson, C.J., 2006. An assessment of the phosphorous retention capacity of wetlands in the Painter Creek Watersched, Minnesota, USA. Water Air and Soil Pollution 171, 169-184.

Brunner, I., Plötze, M., Rieder, S., Zumsteg, A., Furrer, G., Frey, B., 2011. Pioneering fungi fromthe Damma glacier forefield in the Swiss Alps can promote granite weathering. Geobiology 9, 266-279.

Cázares, E., Trappe, J.M., Jumpponen, A., 2005. Mycorrhiza-plant colonization patters on a subalpine glacier forefront as a model system of primary succession. Mycorrhiza 15, 405-416.

Cross, A.F., Schlesinger, W.H., 1995. A literature review and evaluation of the Hedley fractionation: applications to the biogeochemical cycle of soil phosphorus in natural ecosystems. Geoderma 64, 197–214.

Dahms, D. Favilli, F., Krebs, R., Egli, M., 2012. Soil weathering and accumulation rates of oxalate-extractable phases from alpine chronosequences of up to 1 Ma. Geomorphology 151-152, 99-113.

Eger, A., Almond, P.C., Condron, L.M., 2011. Pedogenesis, soil mass balance, phosphorous dynamics and vegetation communities across a Holocene soil chronosequence in a super-humid climate, South Westland, New Zealand. Geoderma 163, 185-196.

Egli, M., Mirabella, A., Fitze, P. 2001. Weathering and evolution of soils formed on granitic, glacial deposits: results from chronosequences of Swiss alpine environments. Catena 45, 19-47.

Egli, M., Fitze, P., 2000. Formulation of pedologic mass balance based on immobile elements: a revision. Soil Science 165, 437-443.

Egli, M., Mirabella, A., Fitze, P. 2003. Formation rates of smectites derived from two Holocene chronosequences in the Swiss Alps. Geoderma 117, 81-98.

Filippelli, G. M., 2008. The global phosphorus cycle: past, present, and future. Elements 4, 89–95.

Finch, A.A., Hole, D.E., Townsend, P.D., 2003. Orientation dependence of luminescence in plagioclase. Physics and Chemistry of Minerals 30, 373-381.

Fitze, P.F. 1982. Zur Relativdatierung von Moränen aus der Sicht der Bodenentwicklung in den kristallinen Zentralalpen. Catena 9, 265-306.

Föllmi, K.B., Hosein, R., Arn, K., Steinmann, P., 2009. Weathering and the mobility of phosphorus in the catchments and foefields of the Rhône and Oberaar glaciers, central Switzerland: Implications for the global phosphorus cycle on glacial-interglacial timescales. Geochimica et Cosmochimica Acta 73, 2252-2282.

Frey, B., Rieder, S.R., Brunner, I, Plötze, M., Koetzsch, S., Lapanje, A., Brandl, H., Furrer, G. 2010. Weathering-Associated Bacteria from the Damma Glacier Forefield: Physiological Capabilities and Impact on Granite Dissolution. Applied and Environmental Microbiology 76, 4788–4796.

Furrer, G. 1991. 25000 Jahre Gletschergeschichte. Neujahrsblatt der Naturforschenden Gesellschaft in Zürich, Orell Füssli, Zürich.

Gamper, M., 1985. Morphochronologische Untersuchungen an Solifluktionszungen, Moränen und Schwemmkegeln in den Schweizer Alpen. Schriftenreihe Physische Geographie, 17, Zürich.

Hindshaw, R.S., Tipper, E.T., Reynolds, B.C., Lemarchand, E., Wiederhold, J.G., Magnusson, J., Bernasconi, S.M., Kretzschmar, R., Bourdon, B., 2011. Hydrological control of stream water chemistry in a glacial catchment (Damma Glacier, Switzerland). Chemical Geology 285, 215-230.

Hitz, C., Egli, M., Fitze, P. 2002. Determination of the sampling volume for representative analysis of alpine soils. Zeitschrift für Pflanzenernährung und Bodenkunde 165, 326-331.

Hoffland, E., Kuyper, T.W., Wallander, H., Plassard, C., Gorbushina, A.A., Haselwandter, K., Holmström, S., Landeweert, R., Lundström, U.S., Rosling, A., Sen, R., Smits, M.M., van Hees P.A.W, van Breemen, N., 2004. The role of fungi in weathering. Frontiers in Ecology and Environment 2, 258–264.

Holzhauser, H., Zumbühl, H., 1996. To the history of the Lower Grindelwald Glacier during the last 2800 years - palaeosols, fossil wood and historical pictorial records - new results. Zeitschrift für Geomorphologie N.F. Suppl. 104, 95-127.

Hosein, R, Arn, K., Steinmann, P., Adatte, T., Föllmi, K.B., 2004. Carbonate and silicate weathering in two presently glaciated, crystalline catchments in the Swiss Alps. Geochimica et Cosmochimica Acta 68, 1021–1033.

Hossner, C.R., 1996. Dissolution for total elemental analysis. In: Sparks, D.L. (Ed.), Methods of Soil Analysis, Part 3, Chemical Methods. Soil Science Society of America Inc. and American Society of Agronomy Inc., Madison, WI, pp. 49–64.

IUSS Working Group WRB. 2007. World Reference Base for Soil Resources 2006, first update 2007. World Soil Resources Reports No. 103. FAO, Rome.

Jann, B., 2005. Einführung in die Statistik. 2., bearbeitete Auflage. Oldenburg Wissenschaftsverlag, München, Germany.

Jongmans, A.G., van Breemen, N., Lundström, U.S., van Hees, P.A.W., Finlay, R.D., Srinivasan, M., Unestam, T., Giesler, R., Melkerud, P.-A., Olsson, M., 1997. Rock-eating fungi. Nature, 389, 682–683.

Kana, J., Kopacek, J., Camarero, L., Garcia-Pausas, J., 2011. Phosphate sorption characteristics of European alpine soils. Soil Science Society of America Journal 75, 862-870.

Keller, C., Védy, J-C., 1994. Distribution of copper and cadmium fractions in two forest soils. Journal of Environmental Quality 23, 987-999.

Kempe, U., Götze, J., 2002. Cathodoluminescence (CL) behaviour and crystal chemistry of apatite from rare-metal deposits. Mineralogical Magazine 66, 151-172.

Kuo, S. 1996. Phosphorus. In: Sparks, D.L. (Ed.), Methods of Soil Analysis, Part 3-Chemical Methods (SSSA Book Series 5). Soil Science Society of America, Madison, pp. 869-919.

Lakanen, E., Erviö, R., 1971. A comparison of eight extractants for the determination of plant-available micronutrients in soil. Acta Agralia Fennica 123, 223-235.

Lichter, J., 1998. Rates of weathering and chemical depletion in soils across a chronosequence of Lake Michigan sand dunes. Geoderma 85, 255-282.

Magny, M., 1992. Holocene lake-level fluctuations in Jura and the northern subalpine ranges, France. Regional pattern and climatic implications. Boreas 21, 319-334.

Maisch, M. 1992. Die Gletscher Graubündens. Rekonstruktion und Auswertung der Gletscher und deren Veränderungen seit dem Hochstand von 1850 im Gebiet der östlichen Schweizer Alpen (Bündnerland und angrenzende Regionen). Teil A: Grundlangen-Analysen-Ergebnisse. Teil B: Verzeichnisse-Datenkataloge-Gletscherkarten. Phys. Geographie 33. Geographisches Institut der Universität Zürich.

Maisch, M., Burga, C.A., Fitze, P. 1993. Lebendiges Gletschervorfeld. Führer und Begleitbuch zum Gletscherlehrpfad Morteratsch. Engadin-Press, Samedan, Switzerland.

Matthews, J.A., Whittaker, R.J., 1987. Vegetation succession on the Storbreen glacier foreland, Jotunheimen, Norway: A review. Arctic and Alpine Research 19, 385-395.

Mavris, C., Egli, M., Plötze, M., Blum, J., Mirabella, A., Giaccai, D., Haeberli, W., 2010. Initial stages of weathering and soil formation in the Morteratsch proglacial area (Upper Engadine, Switzerland). Geoderma 155, 359-371.

Mavris, C., Götze, J., Plötze, M., Mirabella, A., Haeberli, W., Egli, M., 2012. Weathering and mineralogical evolution in a high Alpine soil chronosequence: a combined approach using SEM-EDX, cathodoluminescence (CL) and Nomarski DIC microscopy. Submitted.

Miller, W.P., Martens, D.C., Zelazny, L.W., 1986. Effect of sequence in extraction of trace metals from soils. Soil Science Society of America Journal 50, 598-601.

Neuser, R.D., Bruhn, F., Gätze, F., Haberman, J., Richter, D.K., 1995. Kathodolumineszenz: Methodik und Anwendung. Zentralblatt für Geologie und Paläontologie Teil 1, 287-306.

Nezat, C.A., Blum, J.D., Yanai, R.D., Hamburg, S.P., 2007. A sequential extraction to determine the distribution of apatite in granitoid soil mineral pools with application to weathering at Hubbard Brook Experimental Forest, NH, USA. Applied Geochemistry 22, 2406-2421.

Patzelt, G., 1977. Der zeitliche Ablauf und das Ausmass postglazialer Kimaschwankungen in den Alpen. In Frenzel, B. (ed.), Dendrochronologie und postglaziale Klimaschwankungen in Europa. Erdwiss. Forschung, 13, Wiesbaden, 248-259.

Pearson, F.J., Balderer, W., Loosli, H.H., Lehmann, B.E., Matter, A., Peters, Tj., Schmassmann, H., Gautschi, A., 1991. Applied Isotope Hydrogeology - a case study in northern Switzerland.

Studies in Environmental Science 43, Elsevier, Amsterdam, The Netherlands.

Smith, J.V., 1983. Some chemical properties of feldspars. Mineralogical Society of America, Reviews in Mineralogy 2, 281-296.

Spillmann, P. 1993. Die Geologie des penninisch-ostalpinen Grenzbereichs im südlichen Berninagebirge. Dissertation ETH No.10175, Zürich.

Stott, T., Nuttal, A.-M., Eden, N., Smith, K., Mawell, D., 2008. Suspended sediment dynamics in the Morteratsch pro-glacial zone, Bernina Alps, Switzerland. Geografiska Annaler 90A, 299-313.

Tamburini, F., Bernasconi, S.M., Pfahler, V., Bünemann, E., Frossard, E., 2011. Where life meets rocks: Understanding P cycling during the eraly phases of soil formation. Goldschmidt Conferences Abstract, Mineralogical Magazine, 1983.

van Hees, P.A.W., Rosling, A., Lundström, U.S., Finlay, R.D., 2006. The biogeochemical impact of ectomycorrhizal conifers on major soil elements (Al, Fe, K and Si). Geoderma 136, 364-377.

van Schöll, L., Kuyper, T.W., Smits, M.M., Landeweert, R., Hoffland, E., van Breemen, N., 2008. Rock-eating mycorrhizas: their role in plant nutrition and biogeochemical cycles. Plant and Soil 303, 35–47.

Walker, T.W., Syers, J.K., 1976. The fate of phosphorous during pedogenesis. Geoderma 15, 1-19.

Wallander, H., Hagerberg, D., 2004. Do ectomycorrhizal fungi have a significant role in weathering of minerals in forest soils? Symbiosis 37, 249-257.

Welc M., Bünemann, Frossard E., Jansa J., 2010. Enzymatic activities in the rhizosphere of different plants at a glacier forefield. 19th World Congress of Soil Science, Soil Solutions for a Changing World, pp. 48-51.

White, A.F., Blum, A.E., Bullen, T.D., Vivit, D.V., Schulz, M., Fitzpatrick, J., 1999a. The effect of temperature on experimental and natural chemical weathering rates of granitoid rocks. Geochimica et Cosmochimica Acta 63, 3277-3291.

White, A.F., Bullen, T.D., Vivit, D.V., Schulz, M.S., Clow, D.W., 1999b. The role of disseminated calcite in the chemical weathering of granitoid rocks. Geochimica et Cosmochimica Acta 63, 1939-1953.

Wood, T., Bormann, F.H., Voigt, G.K., 1984. Phosphorous cycling in a northern hardwood forest:

biological and chemical control. Science 223, 391–393.

Zhang, S., Wang, L., Yang, W., 1985. Use of REE analysis in apatite to distinguish petrological and mineralogical series of granitic rocks. Geochimica 1, 45-57.

Table 1

Table 1. Total chemical analysis of the parent material with standard deviation (SD; n=7) in the pro-glacial area.

	Fine earth	SD	Skeleton	SD	Bulk soil	SD
SiO_2 (g/kg)	683.5	97.1	626	52.8	661.6	58.6
CaO (g/kg)	12.1	5.6	37.9	14.7	24.0	8.9
MgO (g/kg)	12.5	5.4	19.1	7.4	15.7	5.3
K_2O (g/kg)	35.9	4.4	33.1	6.3	34.5	4.9
Na_2O (g/kg)	35.0	3.1	38.0	7.4	36.1	4.9
Al_2O_3 (g/kg)	131.1	16.0	156.6	21.8	144.6	12.2
Fe_2O_3 (g/kg)	26.1	7.2	38.0	12.4	32.1	9.8
TiO_2 (g/kg)	11.7	4.3	14.8	5.1	13.3	4.0
MnO_2 (g/kg)	0.7	0.2	0.9	0.2	0.7	0.2
P_2O_5 (g/kg)	1.0	0.4	0.9	0.5	0.9	0.5

Table 2

Click here to download Table: Table2.doc

Table 2. Some physical and chemical properties of the investigated soils.

Site/Soil unit (IUSS, 2006)	Age (yr)	Horizons	Depth (cm)	BD[1)] (g/cm^3)	Skeleton (wt. - %)	Sand[2)] (g/kg)	Silt[2)] (g/kg)	Clay[2)] (g/kg)	pH ($CaCl_2$)	C (g/kg)	Fe_o[3)] (g/kg)	P_{EDTA} (mg/kg)	P_{org} (mg/kg)	P_{inorg} (mg/kg)	P_{tot} (mg/kg)
S1/Humi-Skeletic Leptosol	138	O	0-6	0.2	41	n.m.*	n.m.	n.m.	4.6	321.1	1.028	210	130	333	463
		A	6-9	1.6	50	777	184	39	4.8	6.18	0.635	n.m.	n.m.	n.m.	n.m.
		BC	9-14	1.6	53	830	158	12	4.7	3.69	0.880	n.m.	n.m.	n.m.	n.m.
		C	14-30	1.8	40	757	222	21	4.6	2.8	0.588	n.m.	n.m.	n.m.	311
S2/Humi-Skeletic Leptosol	128	A	0-10	1.4	64	754	204	42	4.85	13.76	1.129	416	514	204	717
		AC	10-40	1.5	68	695	272	33	4.9	4.79	0.975	n.m.	n.m.	n.m.	n.m.
S3/Humi-Skeletic Leptosol	108	A	0-5	1.1	54	667	265	68	5.1	28.1	0.901	224	209	258	466
		AC	5-15	1.7	70	677	281	42	4.5	3.89	1.169	n.m.	n.m.	n.m.	n.m.
S4/Humi-Skeletic Leptosol	98	A/AC	0-5	1.5	53	939	61	15	5.2	14.6	0.414	138	160	173	333
		C	5-30	1.6	70	931	57	12	5.2	1.76	0.347	n.m.	n.m.	n.m.	218
S5/Humi-Skeletic Leptosol	68	A1/A2	0-4	1.3	3	530	432	38	4.85	13.82	0.742	158	154	156	310
		C1	4-9	1.4	36	573	387	40	4.65	2.53	0.583	n.m.	n.m.	n.m.	n.m.
		C2	9-20	1.8	64	570	372	58	4.6	3.65	1.465	n.m.	n.m.	n.m.	n.m.
S6/Skeletic Leptosol	48	A	0-3	1.6	64	n.m.	n.m.	n.m.	4.8	37.47	0.49	0	3	157	160
		C	3-25	1.7	68	852	129	19	5	2.1	0.444	0	0	345	345
S7/Skeletic	48	A	0-4	1.4	26	n.m.	n.m.	n.m.	6.1	60.24	0.371	108	173	629	802

Leptosol														
		C1	4-11	1.6	37	823	146	31	5.2	2.82	0.442	n.m.	n.m.	n.m.	n.m.
		C2	11-34	2.0	67	747	211	42	5.1	3.65	0.616	n.m.	n.m.	n.m.	n.m.
S8/Skeletic Leptosol	58	OA	0-12	1.0	63	n.m.	n.m.	n.m.	4.6	118.2	1.226	247	267	548	815
		C	12-33	1.8	48	712	220	68	4.4	3.12	0.839	n.m.	n.m.	n.m.	880
S9/Humi-Skeletic Leptosol	73	OA	0-10	1.2	59	785	175	40	4.60	47.7	0.755	169	267	355	623
		C	10-36	1.7	58	832	133	35	4.65	3.27	0.741	n.m.	n.m.	n.m.	n.m.
S10/Humi-Skeletic Leptosol	78	A1/A2	0-5	1.3	60	818	143	39	4.6	24.5	0.787	33	134	417	551
		AC	10-25	1.7	84	733	219	48	4.8	4.33	1.334	n.m.	n.m.	n.m.	754
BO1/no soil	1	C	0-5	1.4	73	n.m.	n.m.	n.m.	7.35	n.m.	n.m.	27	0	333	333
B2/no soil	3	C	0-5	1.4	75	n.m.	n.m.	n.m.	7.15	1.9	n.m.	241	13	701	714
B3/Lithic Leptosol	20	(A)C	0-5	1.4	76	n.m.	n.m.	n.m.	6.05	2.9	n.m.	128	0	629	629
B4/Skeletic Leptosol	35	(A)C	0-5	1.4	71	n.m.	n.m.	n.m.	4.95	n.m.	n.m.	24	104	430	535
AP/Albic Podzol	11500	O	0-5	0.8	14	n.m.	n.m.	n.m.	3.3	176.4	0.691	522	551	124	675
		E	5-10	1.3	30	542	375	83	3.3	16.4	0.269	n.m.	n.m.	n.m.	43
		Bs1	15-25	1.5	55	786	184	30	4.4	8.9	1.404	n.m.	n.m.	n.m.	693
		Bs2	40-60	1.7	57	n.m.	n.m.	n.m.	4.7	1.7	0.824	n.m.	n.m.	n.m.	690
		BC	70-80	1.7	53	780	187	33	4.9	0.0	0.391	n.m.	n.m.	n.m.	338
		C	110-120	1.7	67	777	191	32	4.9	0.0	0.336	n.m.	n.m.	n.m.	130

* n.m. = not measured

[1)]BD = bulk density
[2)]Grain sizes: sand (2000-63 μm), silt (63-2 μm) and clay (< 2 μm)
[3)]Oxalate-extractable fraction

Table 3

Table 3. Mineralogical composition of the fine earth fraction (<2mm) of the parent material (t = 0) and the most developed soil horizon (A horizon of a Humi-Skeletic Leptosol (Ranker), t = 138 y) within the proglacial area.

Minerals	Parent material (t = 0) wt.-%	A horizon (t = 138 yr) wt.-%
Quartz	29.1 (±0.8)	30.1 (±0.8)
Albite	27.0 (±1.3)	27.8 (±1.3)
Microcline	11.8 (±0.8)	12.0 (±1.0)
Muscovite	9.4 (±0.7)	10.5 (±0.8)
Epidote	8.0 (±0.7)	6.2 (±0.7)
Hornblende	5.5 (±0.6)	3.9 (±0.5)
Chlorite	1.8 (±0.7)	1.7 (±0.6)
Illite	1.4 (±0.6)	1.9 (±0.6)
Biotite	1.0 (±0.4)	0.7 (±0.5)
Calcite	0.2 (±0.3)	0.6 (±0.3)

Table 4

Click here to download Table: Table4.doc

Table 4. Correlation matrix (Spearman rank correlation coefficient) of the investigated compounds in sources and river waters. The first number designates the correlation coefficient R (e.g. Ca-Mg: 0.91), the second the error probability (e.g. Ca-Mg: <0.01) and the third the number of observations (e.g. Ca-Mg: 95).

	Mg^{2+}	Na^{+}	K^{+}	Sr^{2+}	H^{+}	H_4SiO_4	Cl^{-}	NO_3^{-}	SO_4^{2-}	HCO_3^{-}	Org^{n-}	PO_4^{3-}
Ca^{2+}	0.91 < 0.01 95	0.50 < 0.01 95	0.77 < 0.01 95	0.666 < 0.01 61	-0.45 < 0.01 95	-0.19 0.47 17	0.28 < 0.01 95	0.26 0.01 95	0.63 < 0.01 95	0.52 < 0.01 95	0.57 < 0.01 95	0.60 0.08 9
Mg^{2+}		0.66 < 0.01 95	0.77 < 0.01 95	0.729 < 0.01 61	-0.34 < 0.01 95	-0.15 0.55 17	0.29 < 0.01 95	0.30 < 0.01 95	0.70 < 0.01 95	0.42 < 0.01 95	0.54 < 0.01 95	0.55 0.11 9
Na^{+}			0.47 < 0.01 95	0.57 < 0.01 61	-0.19 0.066 95	0.08 0.76 17	0.27 < 0.01 95	0.35 < 0.01 95	0.64 < 0.01 95	0.27 < 0.01 95	0.31 < 0.01 95	0.15 0.68 9
K^{+}				0.66 < 0.01 61	-0.30 < 0.01 95	-0.01 0.95 17	0.32 < 0.01 95	0.14 0.17 95	0.71 < 0.01 95	0.36 < 0.01 95	0.43 < 0.01 95	0.17 0.64 9
Sr^{2+}					0.18 0.18 61	-0.14 0.59 17	0.52 < 0.01 61	0.51 < 0.01 61	0.73 < 0.01 61	-0.01 0.95 61	0.37 < 0.01 61	-0.25 0.49 9
H^{+}						0.33 0.19 17	-0.05 0.64 95	-0.03 0.78 95	-0.32 < 0.01 95	-0.92 < 0.01 95	0.03 0.74 95	-0.49 0.17 9
H_4SiO_4							0.29 0.25 17	-0.15 0.55 17	-0.01 0.95 17	-0.24 0.34 17	0.28 0.26 17	- - -
Cl^{-}								0.38 < 0.01	0.37 < 0.01	0.07 0.49	0.13 0.21	-0.06 0.84

	95	95	95	95	9
NO_3^-		0.47 < 0.01 95	0.11 0.30 95	-0.12 0.26 95	0.03 0.91 9
SO_4^{2-}			0.38 < 0.01 95	0.16 0.12 95	-0.13 0.71 9
HCO_3^-				-0.14 0.16 95	0.46 0.17 9
Org^{n-}					0.34 0.36 9

Table 5

Table 5. Correlation matrix (Spearman rank correlation coefficient) of the investigated compounds in the soils (fine earth; only pro-glacial area). The first number designates the correlation coefficient R, the second the error probability and the third the number of observations.

	P(org)	P(inorg)	Fe	Al	Si	pH	org. C
P(EDTA)	0.70 < 0.01 15	-0.13 0.63 15	0.78 < 0.01 11	0.31 0.34 11	-0.17 0.60 11	-0.33 0.22 15	0.12 0.68 13
P(org)		-0.32 0.24 15	0.39 0.22 1	0.19 0.56 11	-0.36 0.26 11	-0.44 0.09 15	0.43 0.14 13
P(inorg)			0.00 0.99 11	0.26 0.42 11	0.26 0.416 11	0.49 0.03 15	-0.25 0.39 13
Fe				0.22 0.20 34	0.26 0.144 34	-0.44 < 0.01 34	0.26 0.14 34
Al					0.35 0.04 34	-0.32 0.06 34	0.34 0.05 34
Si						-0.09 0.61 34	-0.30 0.09 34
pH							-0.20 0.24 36

Table 6
Click here to download Table: Table6.doc

Table 6. Total content of some elements in the bulk soil (fine earth and stone fragments up to about a diameter of 200 mm included) of the 11.5 ky-old Podsol outside the pro-glacial area.

Horizon	Depth cm	Fe g/kg	Al g/kg	Na g/kg	K g/kg	P g/kg	Ti g/kg
O	0-5	8.3	40.6	11.3	37.4	0.596	2.48
E	5-10	11.0	57.8	19.3	55.9	0.069	2.80
Bs1	15-25	14.3	68.9	21.3	58.6	0.409	2.78
Bs2	40-60	13.5	66.7	21.2	55.9	0.401	2.76
BC	70-80	11.0	63.6	21.9	58.2	0.254	2.66
C	110-120	13.2	70.3	22.2	58.1	0.162	2.55

Figure 1

Click here to download high resolution image

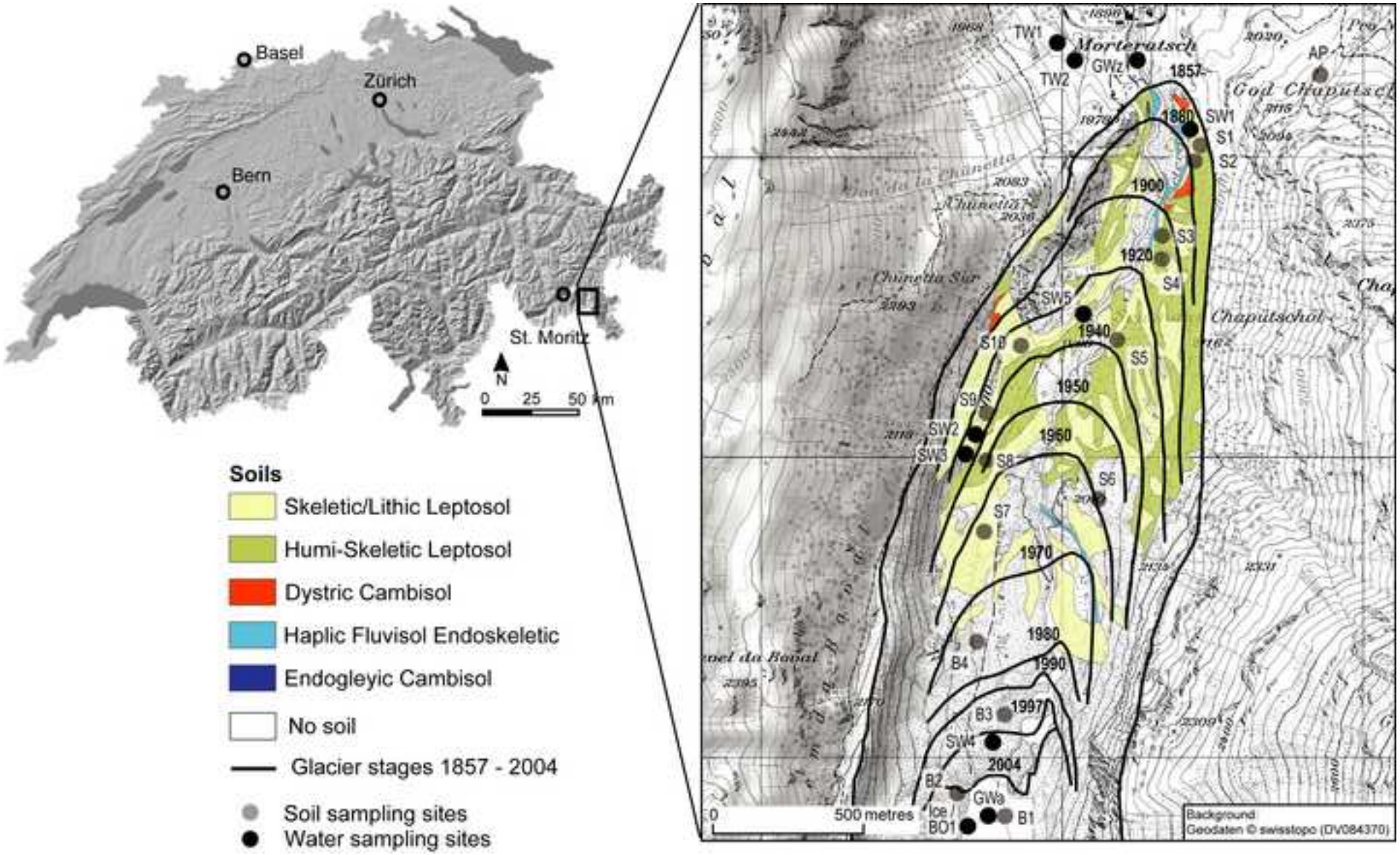

Figure 2

Click here to download high resolution image

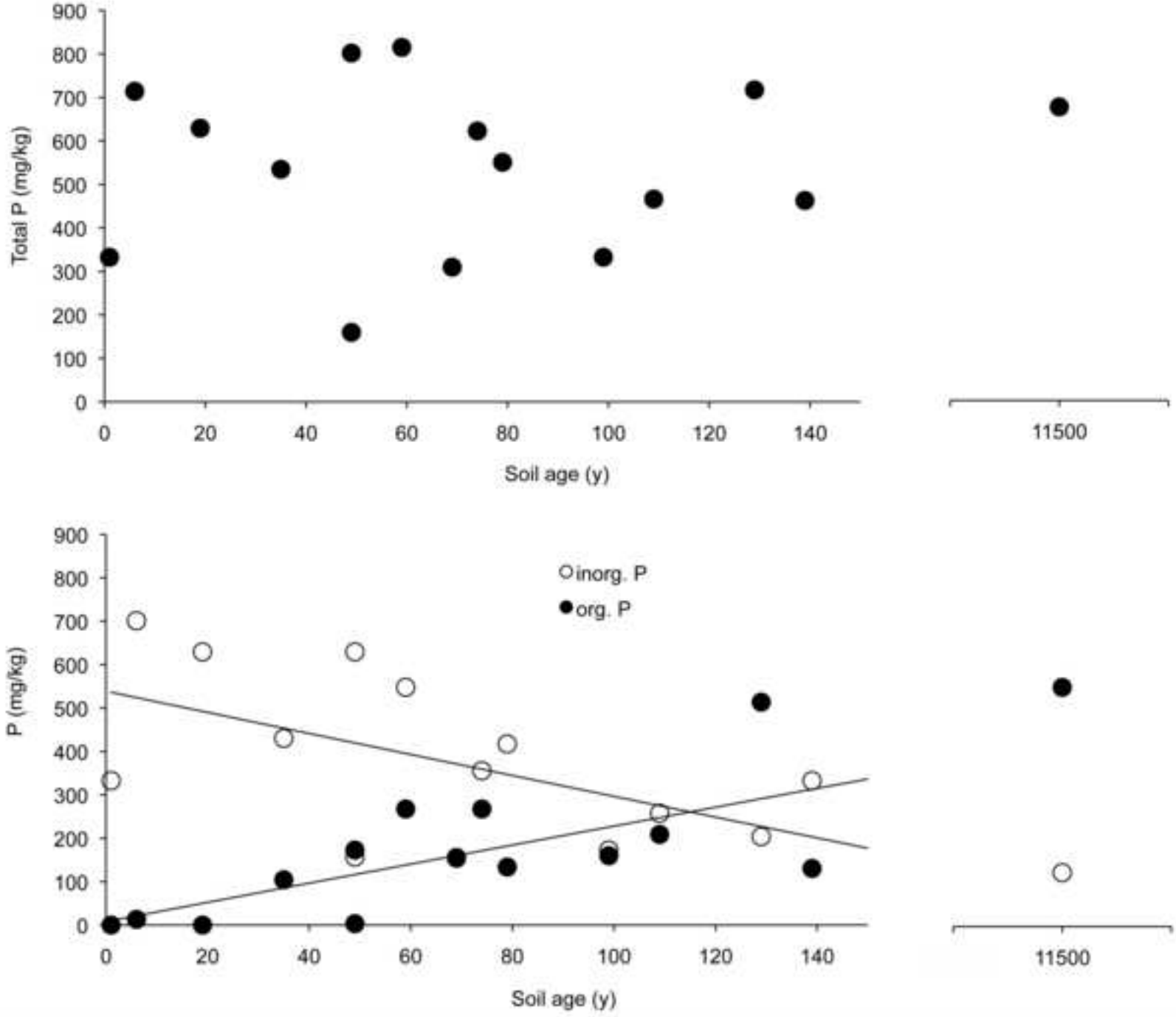

Figure 3

Click here to download high resolution image

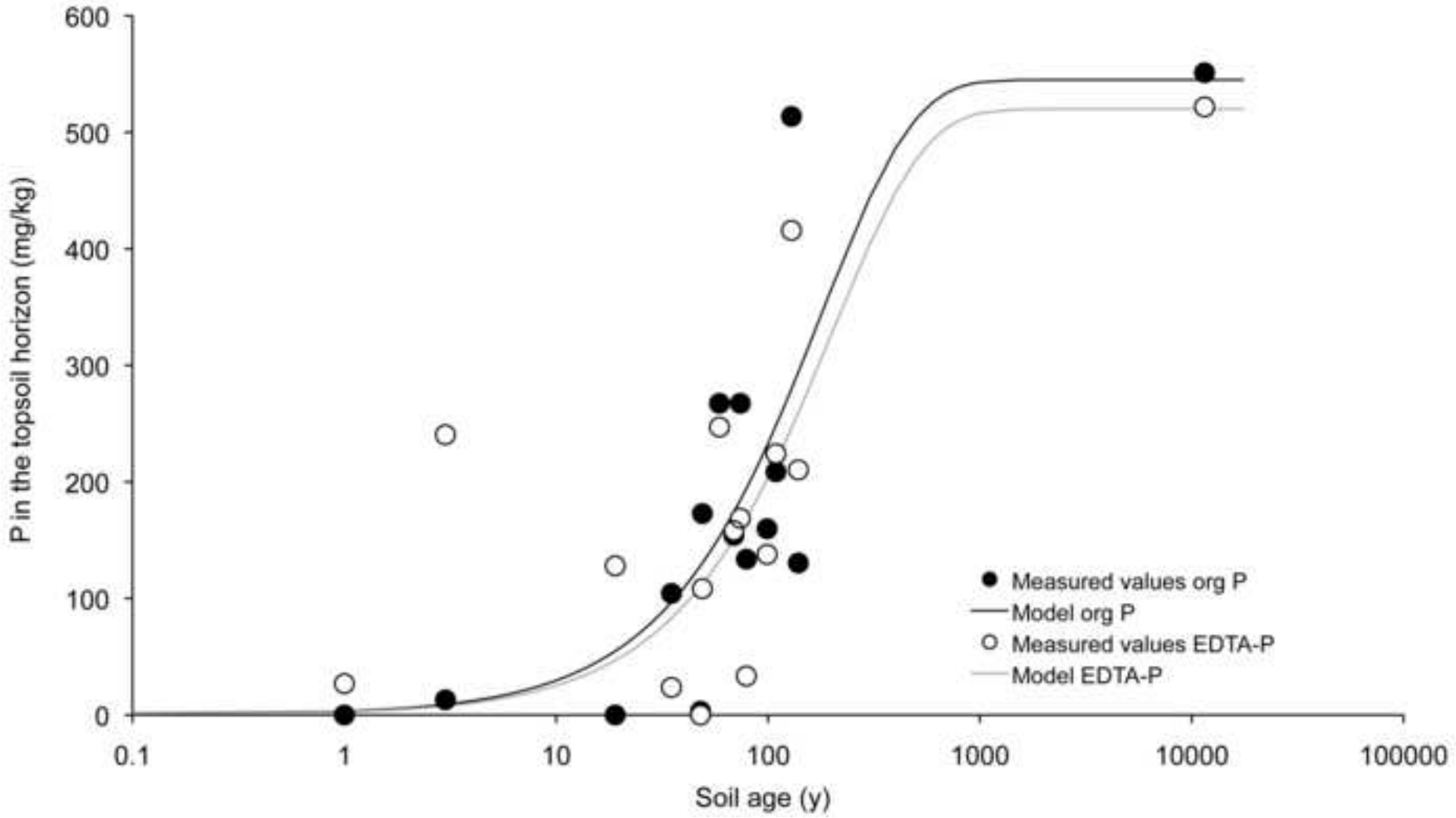

Figure 4

Click here to download high resolution image

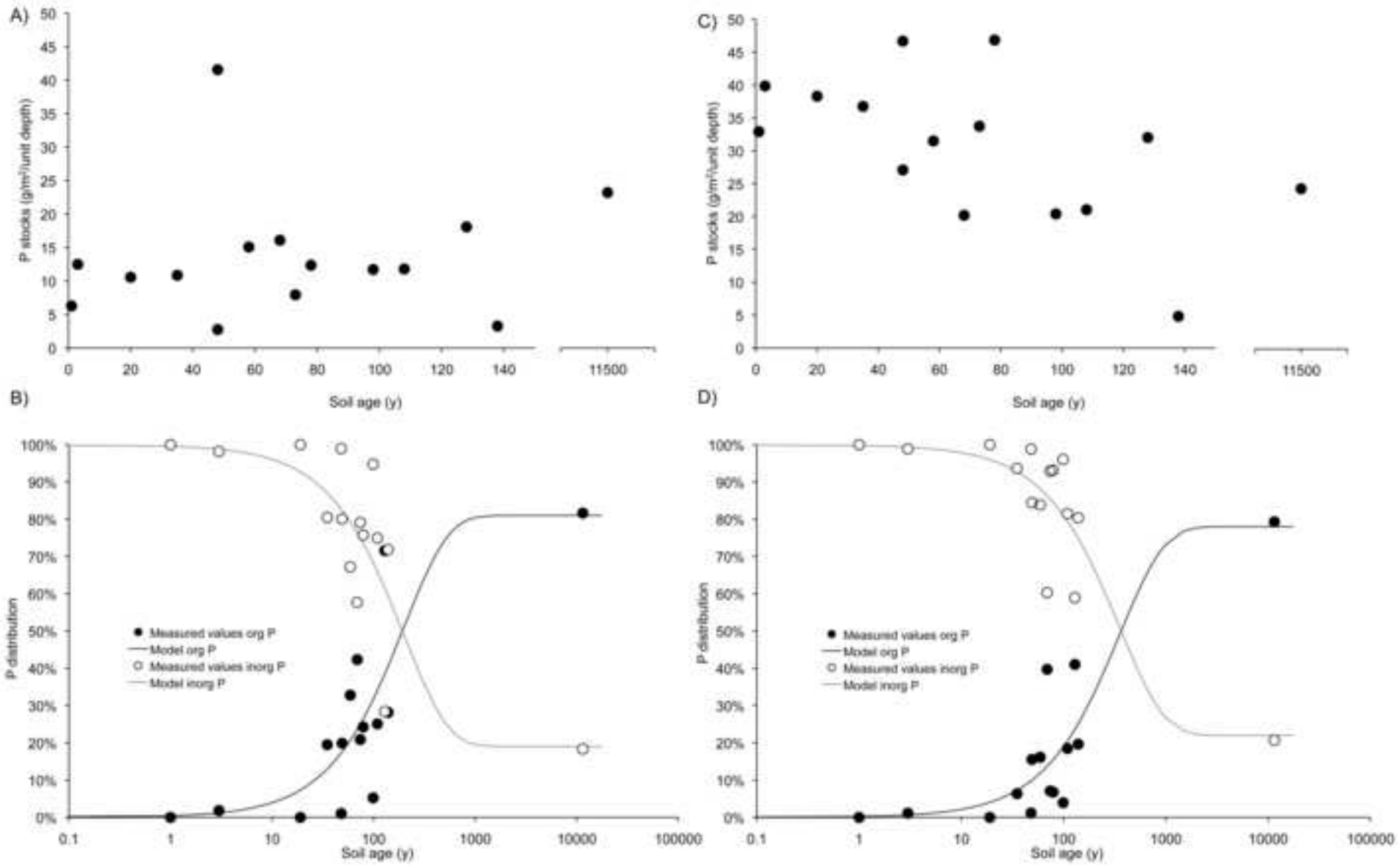

Figure 5

Click here to download high resolution image

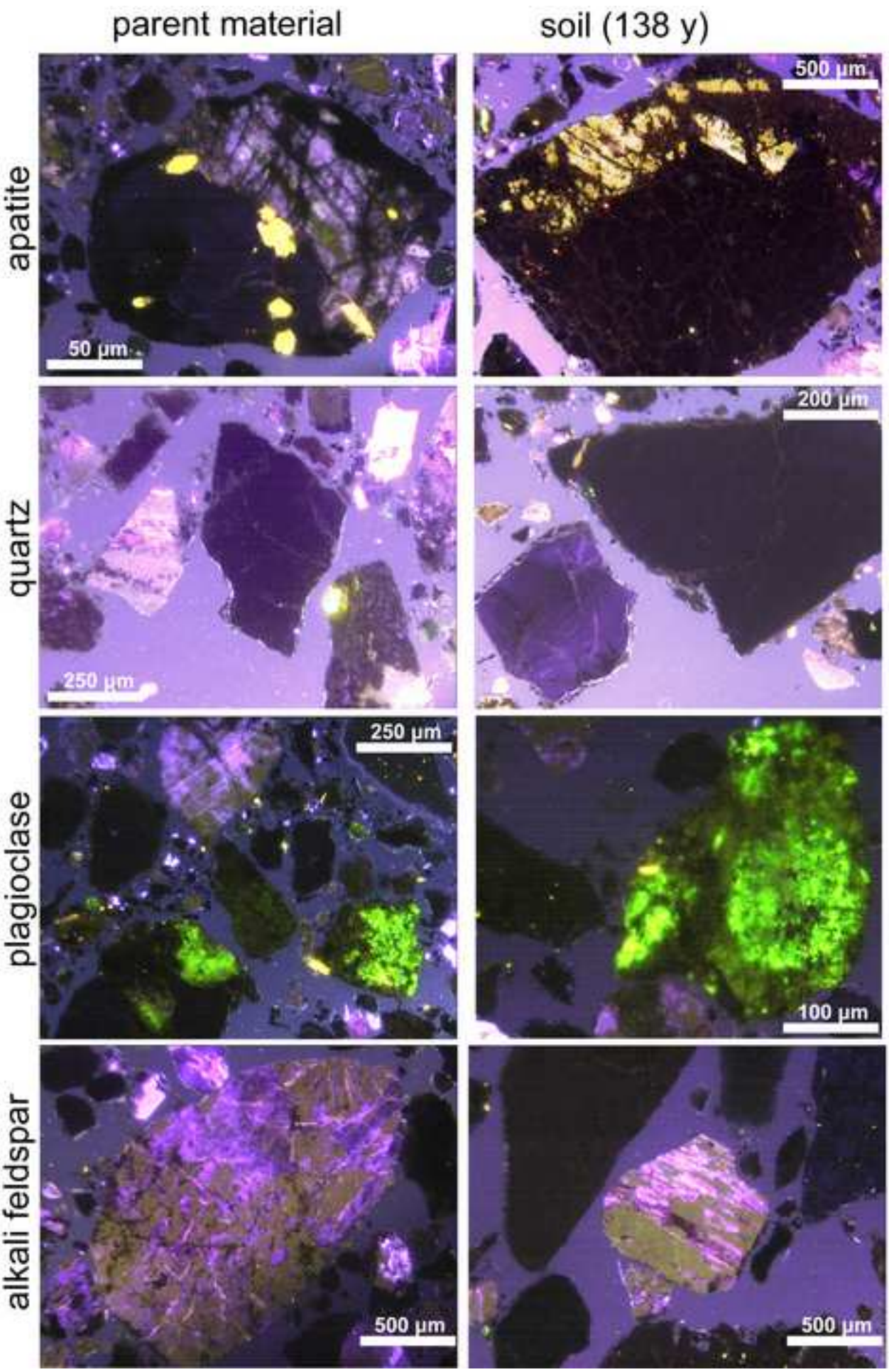

Figure 6

Click here to download high resolution image

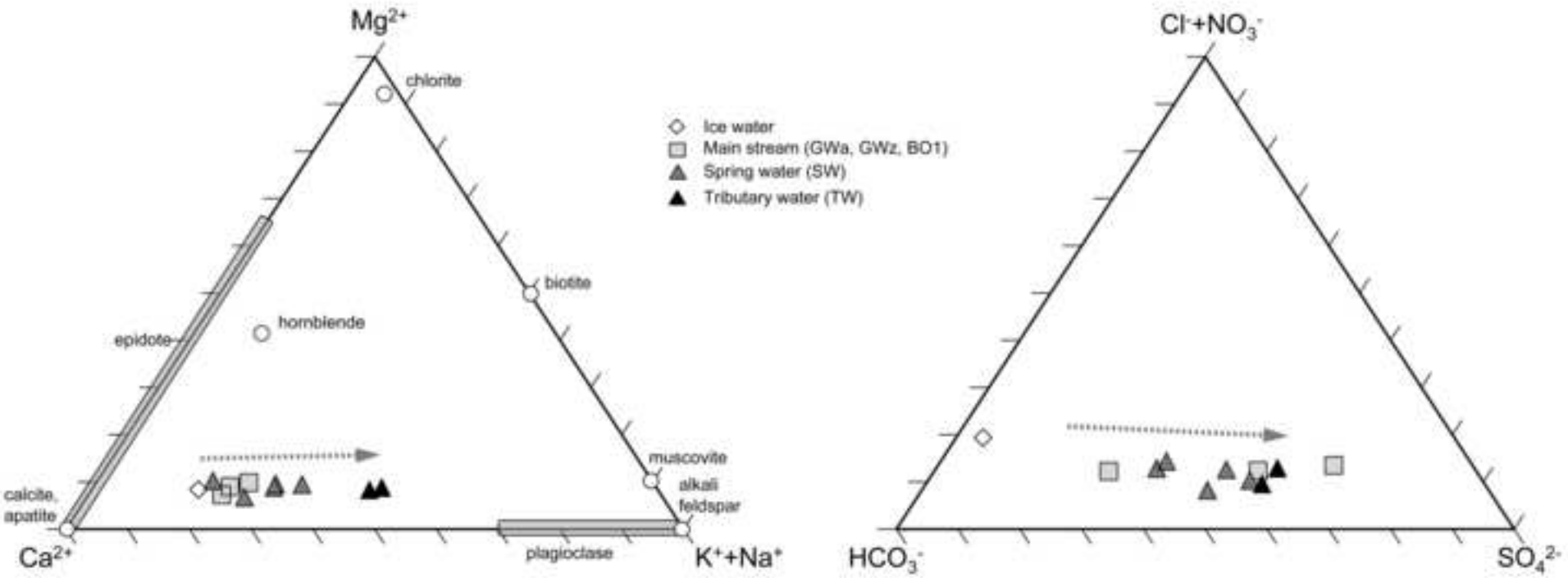

Figure 7
Click here to download high resolution image

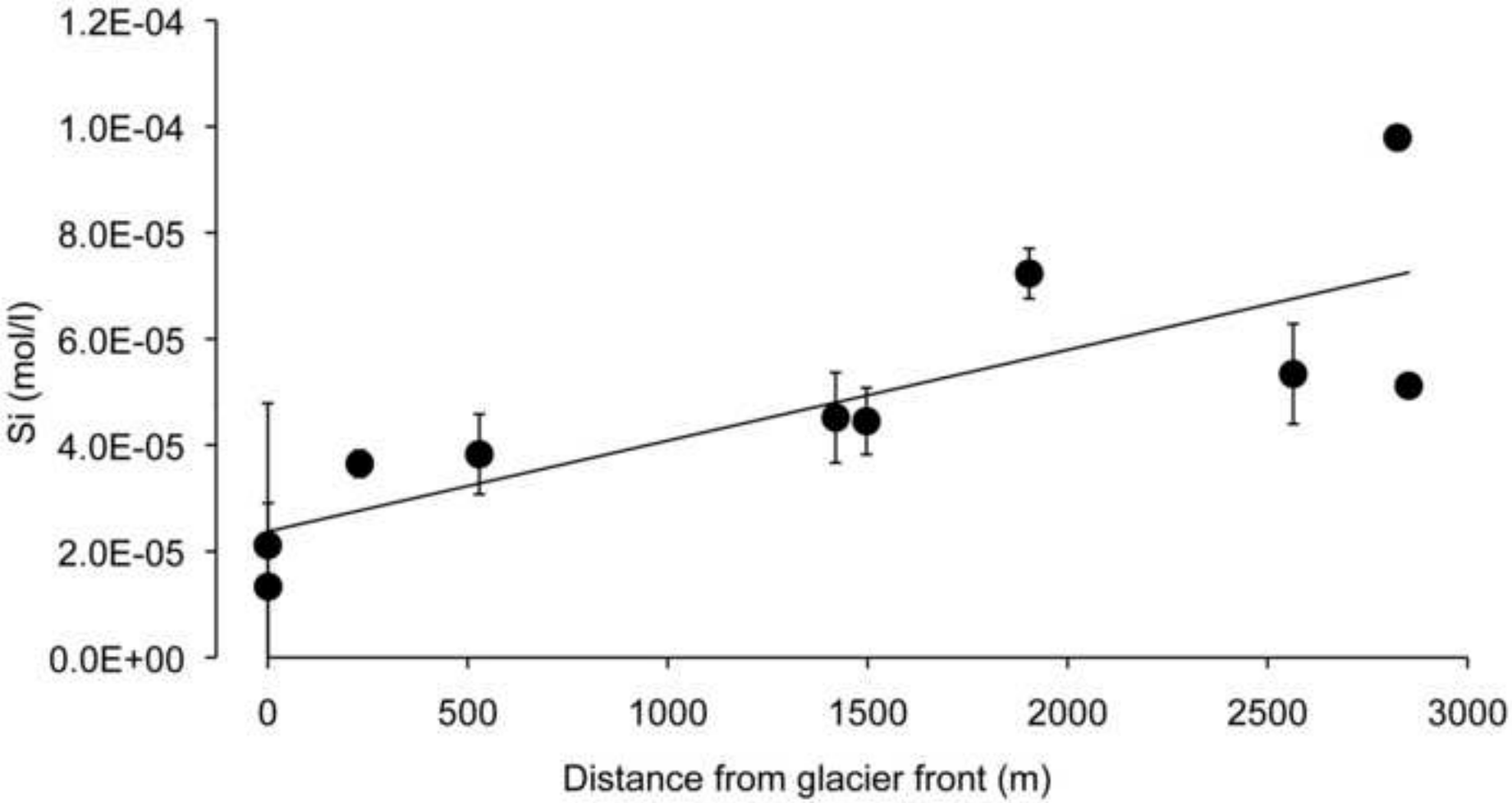

Figure 8

Click here to download high resolution image

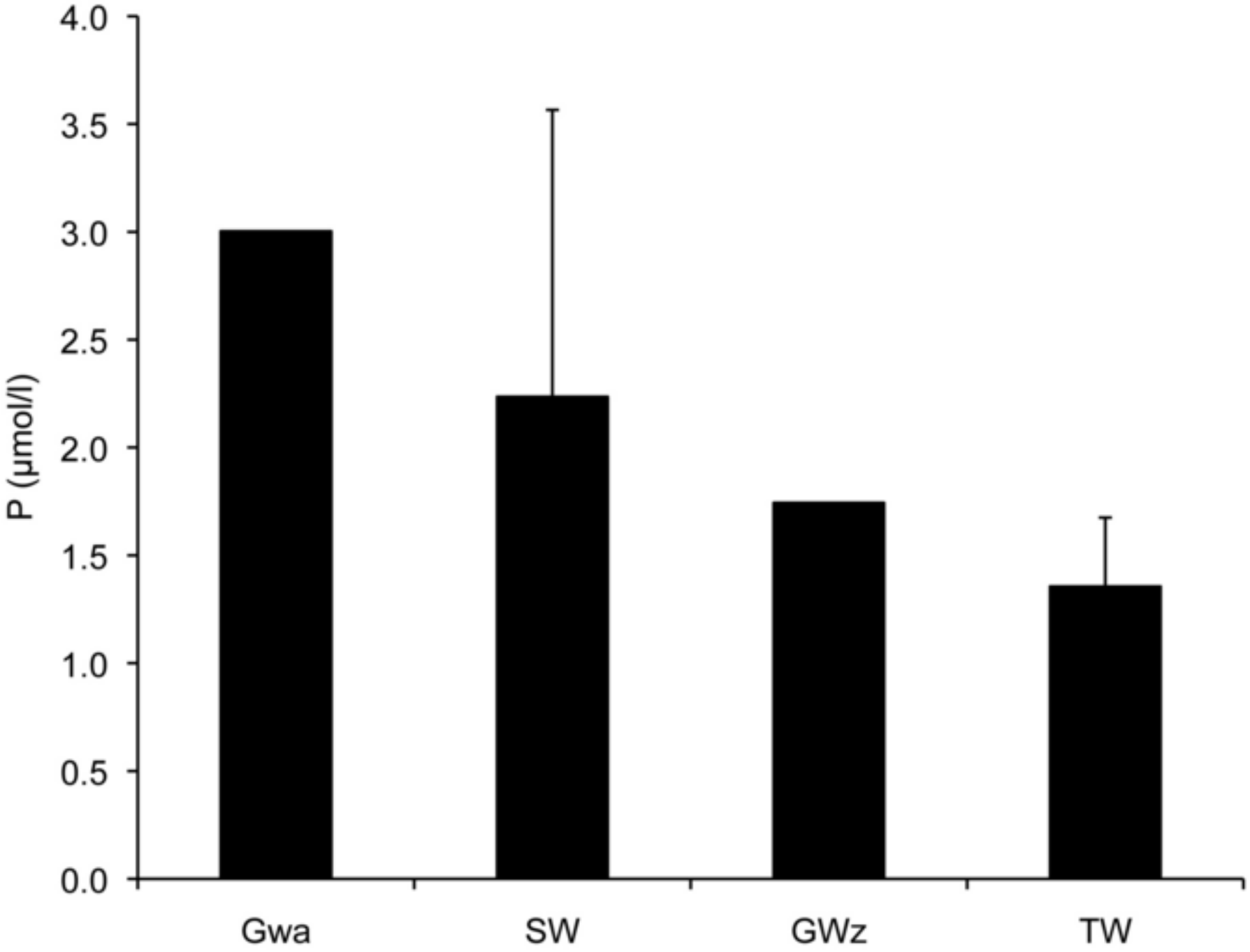

Figure 9

Click here to download high resolution image

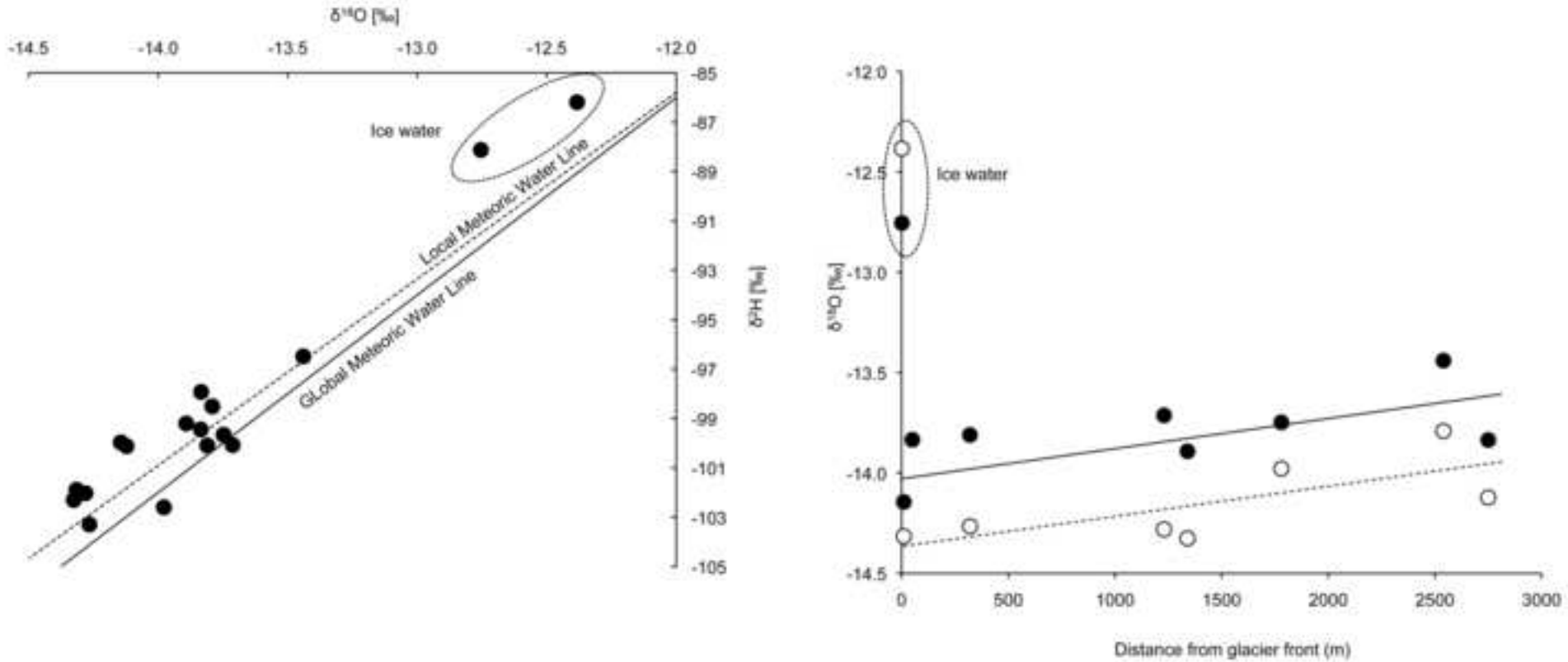

Figure 10

Click here to download high resolution image

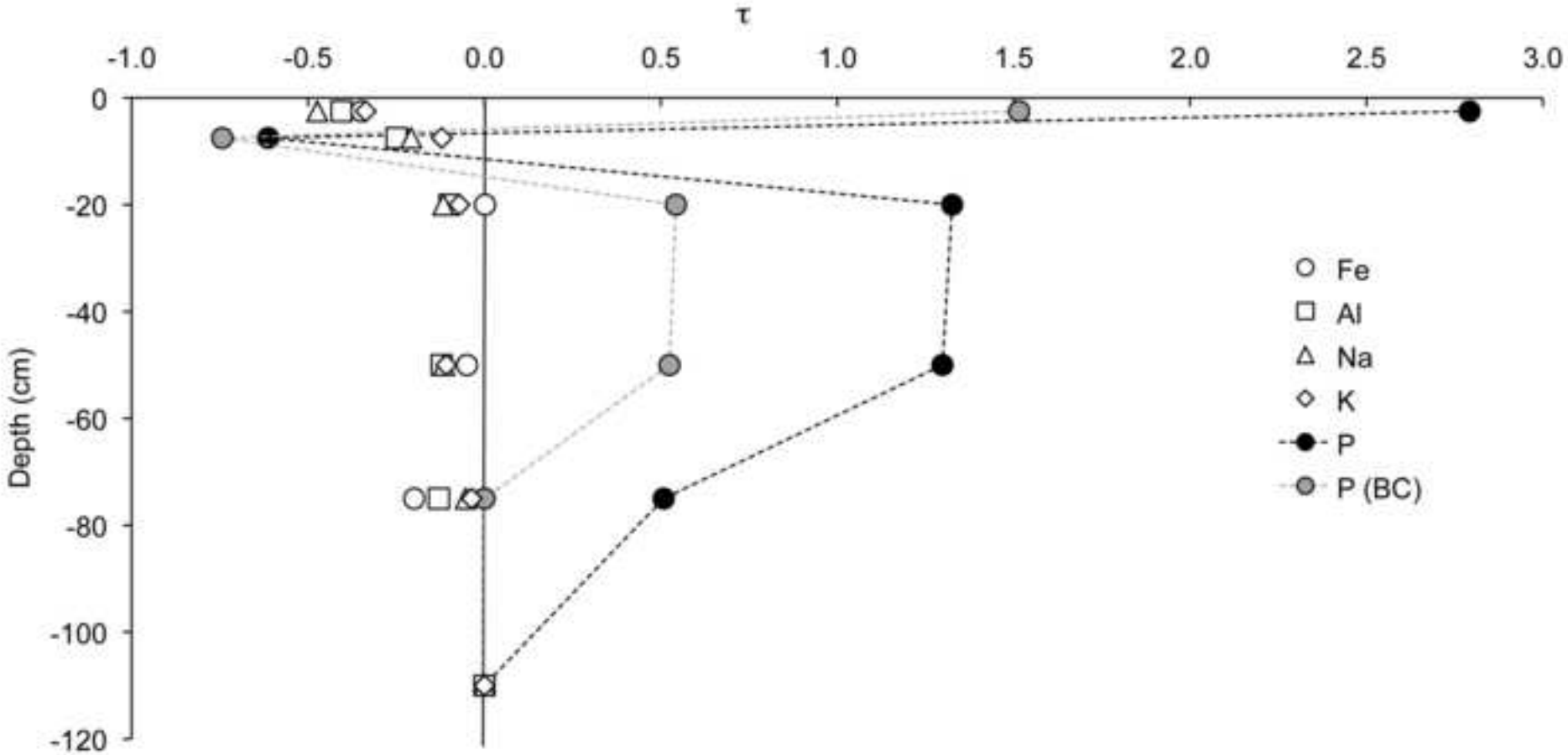

Figure captions

Fig. 1. Location of the Morteratsch forefield with isochrones of glacier retreat, major soil units and position of the topsoil and water sampling sites. SW designates spring waters in the glacier forefield, TW are tributary waters outside the glacier forefield. The other water samples (GWa, GWz, BO1) were taken along the main river. Ice = streamlet on top of the glacier ice.

Fig. 2. Total, inorganic and organic P (fine earth) in the surface horizon of the soils as a function of time (with trend lines for the inorganic and organic P fractions).

Fig. 3. Relationship between EDTA extractable P and organic P. The concentration trend of organic and EDTA-P in the topsoil is modelled using an exponential decay model (see equation 8). The fitting parameters for org. P are: a = 545 mg/kg; b = 0.02 mg/kg; k = 0.00558 y^{-1}, and for the EDTA-P: a = 520 mg/kg; b = 0.05 mg/kg; k = 0.00497 y^{-1}.

Fig. 4. A) P-Stocks (unit depth: 0-5 cm) in the fine earth and B) relative distribution of the P fractions (inorganic and organic P fraction) in the fine earth. C) Total P stocks (including the skeleton fraction; unit depth: 0-5 cm) and D) relative distribution of the inorganic and organic P fraction in the bulk soil (including the soil skeleton). The trend of the relative distributions of the organic and inorganic fractions in B) and D) are modelled using an exponential decay model (see equation 8).
The fitting parameters in B) are: a = 81%; b = 0%; k = 0.0050 y^{-1} for org. P and a = 19%; b = 100%; k = 0.005 y^{-1} for inorg. P and in D) a = 78%; b = 0%; k = 0.0028 y^{-1} for org. P and a = 22%; b = 100%; k = 0.0028 y^{-1} for inorg. P.

Fig. 5. Cathodoluminescence micrographs of apatite, quartz, plagioclase and alkali feldspar of the parent material (0 y) and 138 y old topsoil. Apatite: yellow luminescing crystals due to the activation of Mn^{2+}; quartz: blue-brown CL; plagioclase: green luminescing areas with strongly emitting Mn^{2+} peak;

alkali feldspar: violet emitting grains, related to both Al-O^--Al defects and Fe^{3+} in Al-sites. The heterogeneous internal textures of the feldspar grains are caused by weathering of the material.

Fig. 6. Main chemical composition (mean values) of the analysed waters plotted in ternary diagrams (molar ratios). The dashed arrow shows the temporal evolution. The mineralogical compositions are from Nezat et al. (2007), except for epidote (Armbruster et al., 2006).

Fig. 7. Si concentrations (mean values and SD) in the water as a function of distance from the glacier front.

Fig. 8. Phosphorous concentrations in the waters: GWa = river water near the glacier front, SW = spring water in the glacier forefield, GWz = river water at the end of the glacier forefield, TW = tributary waters outside the glacier forefield.

Fig. 9. Relationship between $\delta^{18}O$ and $\delta^{2}H$ of the waters from the glacier forefield plotted together with the global and local water meteoric line.

Fig. 10. Open-system mass transport function $\tau_{j,w}$ for Fe, Al, Na, K and P as a function of soil depth. Because the variability of the P concentration with soil depth is high, two different variants were calculated: one with the C horizon and another one with the BC horizon as the parent material (i.e. staring point).